

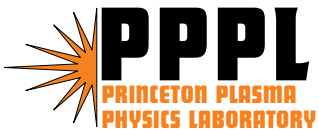
PPPL-4056

PPPL-4056

Low-noise Collision Operators for Particle-in-cell Simulations

J.L.V. Lewandowski

March 2005



PPPL Report Disclaimers

Full Legal Disclaimer

This report was prepared as an account of work sponsored by an agency of the United States Government. Neither the United States Government nor any agency thereof, nor any of their employees, nor any of their contractors, subcontractors or their employees, makes any warranty, express or implied, or assumes any legal liability or responsibility for the accuracy, completeness, or any third party's use or the results of such use of any information, apparatus, product, or process disclosed, or represents that its use would not infringe privately owned rights. Reference herein to any specific commercial product, process, or service by trade name, trademark, manufacturer, or otherwise, does not necessarily constitute or imply its endorsement, recommendation, or favoring by the United States Government or any agency thereof or its contractors or subcontractors. The views and opinions of authors expressed herein do not necessarily state or reflect those of the United States Government or any agency thereof.

Trademark Disclaimer

Reference herein to any specific commercial product, process, or service by trade name, trademark, manufacturer, or otherwise, does not necessarily constitute or imply its endorsement, recommendation, or favoring by the United States Government or any agency thereof or its contractors or subcontractors.

PPPL Report Availability

This report is posted on the U.S. Department of Energy's Princeton Plasma Physics Laboratory Publications and Reports web site in Fiscal Year 2005. The home page for PPPL Reports and Publications is: http://www.pppl.gov/pub_report/

Office of Scientific and Technical Information (OSTI):

Available electronically at: <http://www.osti.gov/bridge>.

Available for a processing fee to U.S. Department of Energy and its contractors, in paper from:

U.S. Department of Energy
Office of Scientific and Technical Information
P.O. Box 62
Oak Ridge, TN 37831-0062
Telephone: (865) 576-8401
Fax: (865) 576-5728
E-mail: reports@adonis.osti.gov

National Technical Information Service (NTIS):

This report is available for sale to the general public from:

U.S. Department of Commerce
National Technical Information Service
5285 Port Royal Road
Springfield, VA 22161
Telephone: (800) 553-6847
Fax: (703) 605-6900
Email: orders@ntis.fedworld.gov
Online ordering: <http://www.ntis.gov/ordering.htm>

Low-noise collision operators for particle-in-cell simulations

J.L.V. Lewandowski*

Princeton Plasma Physics Laboratory

Princeton University, P.O. Box 451

Princeton NJ 08543

USA

(Dated: March 4, 2005)

Abstract

A new method to implement low-noise collision operators in particle-in-cell simulations is presented. The method is based on the fact that relevant collision operators can be included naturally in the Lagrangian formulation that exemplifies the particle-in-cell simulation method. Numerical simulations show that the momentum and energy conservation properties of the simulated plasma associated with the low-noise collision operator are improved as compared with standard collision algorithms based on random numbers.

*Electronic address: jlewando@pppl.gov

I. INTRODUCTION

Marker methods have been used for a long time in various disciplines (*e.g.* plasma physics, astrophysics, etc.) to give numerical solution of purely convective problems [1, 2]. In these methods an ensemble of markers (or ‘superparticles’) is used to approximate the solution; the region of interest covered by the markers defines the phase space associated with the solution. Each marker is represented through its weight and position in phase space. The markers are advanced in time according to the characteristics (‘equations of motion’) of the underlying partial differential equation (PDE) associated with the problem. Marker methods are particularly useful for collisionless problems [1–3, 12]. However, in many applications of interest (*e.g.* turbulent plasmas), collisional processes can have an important impact on the underlying physics. Marker methods usually include collisional effects in a perturbative fashion [4, 5]: in the first step, the markers are evolved in phase space according to the collisionless (*i.e.* purely convective) dynamics; in the second step, drag and diffusion in velocity space are included through a randomization of the markers’ weights and/or velocities according to a prescribed probability distribution. This approach has actually been used for a long time in fluid mechanics; see for example the paper by Chorin [6]. Although the standard method is numerically convenient since it separates the implementation of collisionless dynamics from that of the collisional effects, it also introduces an inherent *noise* because of the ‘velocity randomization’ implied by the method. In this paper, we show that collisional effects can be directly included in the marker trajectories without introducing a randomization mechanism. As mentioned above, the standard method to account for collisions in particle-in-cell (PIC) simulations is reminiscent of the splitting operator method. If f_s denotes the probability distribution function of species s , the collisional Vlasov equation governing f_s can be written as

$$\frac{df_s}{dt} = \sum_{s'} C(f_s, f_{s'}) , \quad (1)$$

where d/dt is the Lagrangian derivative and C is the collision operator. The conventional approach to solve Eq.(1) in PIC simulations is based on the operator splitting method; specifically, Eq.(1) is replaced by the following set of equations:

$$\frac{d\tilde{f}_s}{dt} = 0 , \quad (2)$$

and

$$\frac{\partial f_s}{\partial t} = \sum_{s'} C(\tilde{f}_s, \tilde{f}_{s'}) . \quad (3)$$

Conventional marker methods are appropriate for the collisionless dynamics [Eq.(2)]. However, the collision operator in Eq.(3) usually involves a *diffusive* term in velocity space which is incorporated perturbatively into the dynamics by a randomization of the markers' weights and/or velocities according to a prescribed distribution.

Although this method agrees with physical intuition, it is, from the numerical point of view, quite noisy and possibly inaccurate. The deterministic marker method presented in this paper allows for the *simultaneous* treatment of convective effects [arising from the collisionless dynamics, Eq.(2)] and diffusive effects in velocity space [arising from the collisions, Eq.(3)].

It is worth noting that there has been considerable work done on the topic of collision operators for PIC simulations. In the work of Shanny *et al* [4] electron collisions were modeled as pitch-angle scattering because of the large ion-electron mass ratio; for these collisions momentum conservation is unimportant and it is straightforward to construct and implement Monte Carlo models in which the energy is conserved [4]. For like-particle collisions the issue of momentum and energy conservations is more complex. There are basically two approaches to address the issue. The first approach is based on the linearized Landau collision operator; the drag and diffusion terms are treated the usual way by randomly modifying the positions and velocities of the particles while the particle weights are altered in such a way as to conserve momentum and energy [7, 8]. The second approach, first suggested by Takizuka and Abe [9] and further developed by others [10, 11], is a binary scheme in which the random accelerations and displacements of spatially nearby pairs of particles are correlated such as to conserve the energy and momentum of each pair.

The paper is organized as follows; in section II, a low-noise marker method to treat diffusive processes is described and a numerical example based on the diffusion equation in configuration space is presented. In section III, the noise properties of the deterministic collision operator are compared with that of the standard collision operator (based on a randomization process). One-dimensional simulations of electron plasma waves in presence

of collisions are presented in Section IV; the momentum and energy conservation properties of the simulated plasma for the standard and deterministic collision operators are compared and discussed. Concluding remarks are presented in Section V.

II. MARKER METHOD FOR DIFFUSION EQUATIONS

As mentioned in the Introduction, the main reason for solving the system of equations (2,3) in the conventional PIC method, instead of solving Eq.(1) directly, is the presence of diffusive effects in the collision operator. Therefore, in order to illustrate the new marker method we first consider the one-dimensional diffusion equation (in configuration space)

$$\frac{\partial f}{\partial t} = \frac{\partial^2 f}{\partial x^2} , \quad (4)$$

subject to the initial condition $f_0(x) = f(x, 0)$. The main idea behind the marker method is to write Eq.(4) as a (nonlinear) conservation equation

$$\frac{\partial f}{\partial t} + \frac{\partial}{\partial x} (Vf) = 0 , \quad (5)$$

where

$$V = -\frac{1}{f} \frac{\partial f}{\partial x} . \quad (6)$$

For clarity, $f(x, t)$ is used to denote the exact solution of Eq.(4) whereas $F(x, t)$ represents its approximation. The function f can be approximated by an ensemble of markers (or ‘superparticles’) where each marker j has an associated weight, W_j , and a time-dependent position, $x_j(t)$. As in standard particle methods, such an approximation can be written in terms of delta functions [1, 2]

$$\hat{F} = \sum_{j=1}^N W_j \delta(x - x_j) , \quad (7)$$

where W_j is the weight for marker j and $\delta(x)$ is the usual Kronecker delta function; the hat notation indicates that the representation is singular. For example, $1/\hat{F}(x, t)$ can be singular in region where $f(x, t)$ is nonzero; furthermore, the ratio of delta functions is not defined. Substituting the discrete representation (7) in Eq.(5) yields the characteristics associated with the generalized velocity V

$$\left. \begin{aligned} dx_j/dt &= V(x_j(t), t) \\ x_j(0) &= x_{0j} \end{aligned} \right\} j = 1, \dots, N \quad (8)$$

As noted above, $V \propto \partial \widehat{F} / \partial x / \widehat{F}$ is not well defined. As in conventional particle methods, a smoothed version of \widehat{F} is obtained by taking the convolution of Eq.(7) with a shape function

$$F(x, t) = \left(S_\epsilon \star \widehat{F} \right) (x, t) = \sum_{j=1}^N W_j S_\epsilon(x - x_j) , \quad (9)$$

where $S_\epsilon(x) = S(x/\epsilon)/\epsilon$ and $\int S dx = 1$; ϵ is termed the support parameter. Using representation (9) in the trajectory equations, Eq.(8), one gets

$$\frac{dx_j}{dt} = - \frac{\sum_{k=1}^N W_k S'_\epsilon(x_j(t) - x_k(t))}{\sum_{k=1}^N W_k S_\epsilon(x_j(t) - x_k(t))} \quad (10)$$

where a prime denotes a derivative with respect to the argument and the initial positions are $x_j(0) = x_{0j}$. Note that the weights in Eq.(10) do not vary in time; in particular, if all the weights are initially equal, then all the information about the approximation $F(x, t)$ is contained in the marker positions. The equations of motion (10) can be integrated using standard ordinary differential equation (ODE) techniques, such as the Runge-Kutta method [13], as used in this paper.

Before considering a numerical illustration of the marker method, several observations are in order. Clearly the accuracy of the marker method depends crucially on the shape function and its support parameter, ϵ (see next below). The number of markers, the method of integration of the equations of motion, the initial loading of the ensemble $\{(x_k, W_k); k = 1, \dots, N\}$ and the time step of integration are parameters that also influence the accuracy of the marker method. In some sense, the positions of the markers define a moving grid as far as the approximate solution is concerned. Of course one can reconstruct the approximate solution F on a fixed grid $\{X_g; g = 1, \dots, N_g\}$ at time t by invoking the representation (9):

$$F_g(t) = F(X_g, t) = \sum_{j=1}^N W_j S_\epsilon(X_g - x_j(t)) .$$

As mentioned earlier, the accuracy of the marker method depends crucially on the properties of the smoothed PDE's approximate solution. Therefore it is important to study the impact of the shape function and its support parameter ϵ on test functions. As it will become

apparent below, the accuracy of the smoothing approximation is also related to the initial loading of the markers. The smoothed approximation of the exact solution $f(x)$ is given by

$$F(x) = \sum_{j=1}^N W_j S_\epsilon(x - x_j) , \quad (11)$$

where $S_\epsilon(x) = S(x/\epsilon)/\epsilon$ and the shape function $S(x)$ with finite support satisfies the normalization condition

$$\int_{-1}^{+1} S(x) dx = 1 ,$$

and $S(x) = 0$ for $|x| > 1$. In some cases, there are advantages in using shape functions with infinite support, in which case the normalization condition is of the form $\int_{-\infty}^{+\infty} S dx = 1$. Apart from the actual form of the shape function, there is some freedom in selecting the value of the support parameter ϵ . However one can estimate an appropriate value for ϵ based on the following considerations. For illustrative purposes, consider a simulation with N markers that are initially distributed uniformly in the interval $x \in [-L, L]$; therefore, at $t = 0$, the average distance between markers is $h = 2L/N$. If the support parameter is such that $\epsilon < h$, then $S_\epsilon(x_j - x_k) \propto S((x_j - x_k)/\epsilon) = 0$ for all markers $j \neq k$; this implies that the position of each marker will be independent of the positions of the other markers at least at $t = 0$. We conclude that the support parameter must be larger than the average distance between markers, at least in the average sense. In addition, the value of ϵ , which is akin to a grid spacing in the finite difference method, must be chosen such as to accurately resolve the spatial scale length of $f(x)$. In summary, if λ denotes the (known or estimated) spatial scale length of $f(x)$ and h is the average distance between markers, the support parameter, ϵ , must satisfy the following inequality

$$h \ll \epsilon \ll \lambda .$$

There is some freedom in selecting a shape function. Typically one requires some smoothness properties and/or ease of computation (for example, a Gaussian shape function is smoother than a hat shape function, but it is computationally more demanding to evaluate). Below

is a set of shape functions that are defined on the interval $[-1, +1]$:

$$\begin{aligned}
S_1(x) &= \frac{1}{2} \quad (\text{gate function}) \\
S_2(x) &= 1 - |x| \quad (\text{hat function}) \\
S_3(x) &= \frac{3}{4} (1 - x^2) \quad (\text{quadratic polynomial}) \\
S_4(x) &= \frac{15}{16} (1 - x^2)^2 \quad (\text{quartic polynomial}) \\
S_5(x) &= \mu (1 - |x|) e^{-x^2} \quad (\text{hat/Gaussian shape function}) \\
S_6(x) &= \beta (1 - x^2)^2 e^{-x^2} \quad (\text{quartic polynomial/Gaussian shape function})
\end{aligned} \tag{12}$$

where $\mu = (\sqrt{\pi} \text{erf}(1) + 1/e - 1)^{-1}$ and $\beta = 2 / (\frac{3}{2} \text{erf}(1) - 1/e)$ are constants of normalization, and $\text{erf}(x)$ denotes the error function

$$\text{erf}(x) = \frac{2}{\sqrt{\pi}} \int_0^x e^{-t^2} dt .$$

The second factor that affects the approximation of $f(x)$ is the initial distribution of the position of the markers and their associated weights (referred to as the initial loading). There are two basic approaches to the initialization of the ensemble $\{(x_j, W_j) ; j = 1, \dots, N\}$. In the first approach, the markers are uniformly distributed in space. Using the approximation of

$$\int f(x) dx \approx \sum_j f(x_j) h ,$$

where h is the distance between two neighboring markers, and noting that [see Eq.(7)]

$$\int \hat{F} dx = \sum_j W_j ,$$

it follows that

$$\begin{aligned}
W_j &= f(x_j) h , \\
x_{j+1} - x_j &= h .
\end{aligned}$$

In the second approach, each marker has the same weight, but the spatial distribution of the markers is not uniform. If there are N markers, the marker weight is then $W_j = \sigma/N$ where $\sigma \equiv \int_{-\infty}^{+\infty} f dx$. In order to determine the spatial distribution of the markers, it is convenient to introduce the variable

$$\xi = \frac{\int_{-\infty}^x f(x') dx'}{\int_{-\infty}^{+\infty} f(x) dx} ,$$

which, by construction, is a positive-definite quantity in the unit interval. A uniform distribution in ξ , that is $\xi_j = (j - \frac{1}{2})/N$ ($\forall j$), yields

$$\begin{aligned} x_j &= g^{-1} \left(\left(\int_{-\infty}^{+\infty} f(x) dx \right) \frac{j - \frac{1}{2}}{N} \right) , \\ W_j &= \frac{\sigma}{N} , \end{aligned} \quad (13)$$

where g^{-1} denotes the inverse of $g(x) \equiv \int_{-\infty}^x f(x') dx'$. As a numerical illustration, consider the function

$$f(x) = x e^{-x^2} ,$$

in the interval $x \in [0, x_0]$, $x_0 > 0$. The initialization based on a set of uniformly distributed x_j yields

$$\begin{aligned} x_j &= (j - 1/2)h , \\ W_j &= x_j e^{-x_j^2} h , \end{aligned}$$

where $h = x_0/N$. Alternatively, one can demand that each marker carries an equal weight; following the procedure described above [Eq.(13)] one obtains

$$\begin{aligned} x_j &= \sqrt{-\ln \left(1 - \frac{j - 1/2}{N} (1 - e^{-x_0^2}) \right)} , \\ W_j &= \frac{1}{N} . \end{aligned} \quad (14)$$

Fig.1 shows the smoothed approximation of $f(x)$ for a uniform spatial loading (dotted line) and a nonuniform spatial loading (dashed line) using a quadratic shape function with support parameter $\epsilon = 0.1$ for a set of $N = 32$ markers. The plain line represents the exact function. For the same parameters, the quartic shape function, which satisfies $S'(x = \pm 1) = 0$, yields a better approximation (Fig. 2). Further improvement (Fig. 3) can be achieved using the shape function based on a quartic polynomial and a Gaussian function [$S(x) = S_6(x)$; see Eq.(12)]. Of course, in all the above cases, smoother approximations can be obtained by increasing the number of markers N . Another parameter affecting the accuracy of the approximation is the support parameter, ϵ . Fig. 4 is the same as Fig. 2 except that the support parameter has been doubled ($\epsilon = 0.2$). Clearly a much better agreement between the approximated functions and the exact function is found. If the support parameter is

further increased the smoothing effect of $S(x)$ becomes too important and the accuracy of the approximated function degrades.

We now apply the marker method to the diffusion equation, Eq.(4), with initial conditions

$$\left. \begin{aligned} f_0(x) &= 1 ; |x| \leq 1 \\ &= 0 ; |x| > 1 \end{aligned} \right\} \quad (15)$$

The solution of the diffusion equation, Eq.(4), with initial conditions (15) is easily found using Laplace transforms

$$\begin{aligned} f(x, t) &= \frac{1}{\sqrt{4\pi t}} \int_{-\infty}^{+\infty} f_0(\xi) \exp(-(x - \xi)^2/4t) d\xi \\ &= \frac{1}{2} \left[\operatorname{erf}\left(\frac{x+1}{2\sqrt{t}}\right) - \operatorname{erf}\left(\frac{x-1}{2\sqrt{t}}\right) \right], \end{aligned}$$

where, as before, $\operatorname{erf}(x)$ is the error function with argument x . As mentioned in the previous section, there is some freedom in the choice of the shape function $S(x)$. Here we consider a shape function with infinite support (superGaussian)

$$S_7(x) = \frac{3/2 - x^2}{\sqrt{\pi}} e^{-x^2}. \quad (16)$$

The equations of motion (10) have been integrated using a second-order Runge-Kutta method with a fixed time step. The approximate solution has been reconstructed on a moving grid defined by the marker positions $\mathbf{x}(t) = \{x_j(t); j = 1, \dots, N\}$. Note that one can determine the approximate solution on a fixed, prescribed grid; however this approach involves the shape function (or some other form of interpolation) that further reduces the accuracy of the numerical scheme. Fig. 5 shows the exact solutions (plain line: $t = 2.0$; dotted line: $t = 4.0$) and the approximate solutions (triangles: $t = 2.0$; squares: $t = 4.0$) of the diffusion equation for a set of $N = 100$ markers. The initial condition is the square profile of Eq.(15). The shape function is a superGaussian [Eq.(16)]; other parameters are $\Delta t = 0.01$, $\epsilon = 1/3$ and $L = 14.0$. We note the excellent agreement of the approximate solutions with the exact solutions. As it can be expected, slight errors do appear when $F \mapsto 0$ although their magnitude are small.

III. NOISE PROPERTIES OF A MODEL COLLISION OPERATOR

In this Section, we apply the new marker method to a model collision operator. In particular, the collisional relaxation of a given probability distribution function towards a Maxwellian distribution function is considered. The marker method is compared with the conventional method based on the Monte Carlo method (randomization of the marker velocities).

A. Deterministic Collision Operator

Our model problem is given by

$$\frac{\partial f}{\partial t} = C(f) , \quad (17)$$

where the collision operator is (in appropriate normalized units; see next section)

$$C(f) = \underbrace{\nu_{ei} \frac{\partial^2 f}{\partial v^2}}_{\mathbf{1}} + \underbrace{\nu_{ei} \frac{\partial}{\partial v} (vf)}_{\mathbf{2}} , \quad (18)$$

where term **1** represents the diffusive component of C and term **2** accounts for the drag; ν_{ei} is a (constant) basic collision frequency. The collision operator (18) annihilates a Maxwellian distribution, $C(f_M) \equiv 0$, where $f_M = \exp(-v^2/2) / \sqrt{2\pi}$. Following the methodology described in the previous section, Eq.(17) can be written as a conservation equation

$$\frac{\partial f}{\partial t} + \frac{\partial}{\partial v} (\mathcal{D}f) = 0 ,$$

where

$$\mathcal{D} = -\frac{1}{f} \int_{-\infty}^v C(f(v')) dv' = -\nu_{ei} \left(\frac{1}{f} \frac{\partial f}{\partial v} + v \right) . \quad (19)$$

As before, f is approximated by its discrete representation F based on a set of N markers:

$$F(v, t) = \sum_{k=1}^N W_k S_\epsilon(v - v_k(t)) .$$

The marker trajectories are given

$$\left. \begin{aligned} dv_j/dt &= -\nu_{ei} \left[\frac{\sum_{k=1}^N W_k S'_\epsilon(v_j - v_k)}{\sum_{k=1}^N W_k S_\epsilon(v_j - v_k)} + v_j \right] , \\ v_j(0) &= v_{0j} , \end{aligned} \right\} j = 1, \dots, N \quad (20)$$

where a prime denotes a derivative with respect to the argument. Eqs.(20) can be integrated using standard ODE techniques (*e.g.* Runge-Kutta algorithm).

B. Monte Carlo Collision Operator

In this Section, the conventional PIC approach for the solution of Eq.(17) is presented. For simplicity, we derive an equivalent Monte Carlo collision operator based on the binomial distribution. Let us define the velocity moment of order ℓ as

$$\langle v^\ell \rangle \equiv \int_{-\infty}^{+\infty} v^\ell f dv .$$

Multiplying Eq.(17) by v and v^2 and integrating over velocity space, one gets

$$\begin{aligned} \frac{d\langle v \rangle}{dt} &= -\nu_{ei} \langle v \rangle , \\ \frac{d\langle v^2 \rangle}{dt} &= 2\nu_{ei} (1 - \langle v^2 \rangle) . \end{aligned}$$

It follows from the above expressions that the variance of f defined as $\sigma^2 \equiv \langle v^2 \rangle - \langle v \rangle^2$ evolves in time according to

$$\frac{d\sigma^2}{dt} = 2\nu_{ei} (1 + \langle v \rangle^2 - \langle v^2 \rangle) .$$

If at $t = 0$ the distribution function is a delta function around v_0 , $f = \delta(v - v_0)$, and noting that (at $t = 0$)

$$\begin{aligned} \frac{d\langle v \rangle}{dt} &= -\nu_{ei} v_0 , \\ \frac{d\sigma^2}{dt} &= 2\nu_{ei} , \end{aligned}$$

then, after a short time Δt , we expect f to be a Gaussian centered at $v = v_0 - \nu_{ei} v_0 \Delta t$ with standard deviation $\sqrt{2\nu_{ei} \Delta t}$. In other words, if $v(v^*)$ denotes the marker velocity before (after) the collision, we have the relation of

$$v^* = (1 - \nu_{ei} \Delta t) v \pm \sqrt{2\nu_{ei} \Delta t} ,$$

or

$$v^* = (1 - \nu_{ei} \Delta t) v + [2H(\xi - \frac{1}{2}) - 1] \sqrt{2\nu_{ei} \Delta t} , \quad (21)$$

where $H(x)$ is Heaviside function with argument x and ξ is a random number uniformly distributed between 0 and 1.

C. Numerical Comparison

In this Section, we study the collisional relaxation of an initial square distribution

$$f(v, 0) \equiv f_0(v) = \left. \begin{aligned} &= 1 ; |v| \leq 0.5 \\ &= 0 ; |v| > 0.5 \end{aligned} \right\}$$

using the deterministic marker method [Eq.(20)] and the Monte Carlo method [Eq.(21)]. In the limit of an infinite number of markers, we expect both methods to yield the exact steady state solution. However, from the practical point of view, the relevant quantity is the difference between the approximate and exact solutions for finite (and possibly small) N . Fig.6 shows the collisional relaxation of an initial square distribution function (plain line) towards a Maxwellian distribution (dashed line) using the Monte Carlo method. The dotted line represents the distribution function after 30 collision times. The simulation has been carried out using a set of $N = 200$ markers, a time step of $\Delta t = 0.1$ and a collision frequency of $\nu_{ei} = 0.5$. The distribution function has been reconstructed on a fixed grid on the interval $v \in [-3, +3]$ with $N_g = 500$ grid points. The most striking aspect of Fig. 6 are the large local deviations of the simulated distribution function; of course, the amplitude of these deviations can be reduced by increasing the number of markers for an additional computational cost. Fig. 7 depicts the same quantities as in Fig.6 except that the deterministic collision operator has been used here. The initial conditions and the parameters are the same as those of Fig.6. The distribution function is in excellent agreement, excepts perhaps for small deviations for large v (where F turns out to be small). Fig. 8 presents an alternative perspective of Fig. 7. The triangles represent the actual position of the markers after 30 collision times. The bulk of the distribution function is in excellent agreement with the Maxwellian distribution.

IV. LOW-NOISE PARTICLE-IN-CELL SIMULATIONS

In the previous Section, it has been shown that, for a given number of markers, the deterministic marker method is much more accurate than the conventional Monte Carlo method. The aim of this section is to demonstrate that the use of a deterministic collision operator yields better momentum and energy conservation properties as compared to the case of a Monte Carlo collision operator. We consider a one-dimensional periodic system of period L with a uniform background of cold ions. The electron distribution function obeys

the equation of

$$\frac{\partial f}{\partial t} + v \frac{\partial f}{\partial x} + \frac{e}{m_e} \frac{\partial \Phi}{\partial x} \frac{\partial f}{\partial v} = C(f),$$

where

$$C(f) = \nu_{ei} \left(V_{th}^2 \frac{\partial^2 f}{\partial v^2} + \frac{\partial}{\partial v} (fv) \right).$$

Here m_e is the electron mass, $V_{th} = \sqrt{T_e/m_e}$ is the electron thermal velocity and Φ is the electrostatic potential which can be determined from the Poisson equation, $\partial^2 \Phi / \partial x^2 = 4\pi e(n_e - n_i)$. In normalized units ($x/\lambda_D \mapsto x$, $\lambda_D = \sqrt{T_e/(4\pi e^2 n_0)}$ is the Debye length, n_0 is the background density, $\omega_p t \mapsto t$, $\omega_p = V_{th}/\lambda_D$ is the electron plasma frequency, $fV_{th}/n_0 \mapsto f$, $e\Phi/T_e \mapsto \Phi$, $\nu_{ei}/\omega_p \mapsto \nu_{ei}$), the following system of equations is obtained

$$\frac{\partial f}{\partial t} f + v \frac{\partial f}{\partial x} + \frac{\partial \Phi}{\partial x} \frac{\partial f}{\partial v} = C(f), \quad (22)$$

where

$$C(f) = \nu_{ei} \left(\frac{\partial^2 f}{\partial v^2} + \frac{\partial}{\partial v} (fv) \right), \quad (23)$$

and

$$\frac{\partial^2 \Phi}{\partial x^2} = \int_{-\infty}^{+\infty} f dv - 1. \quad (24)$$

Using the results of the previous section, we can write Eq.(22) in a *full* conservative form

$$\frac{\partial f}{\partial t} + \frac{\partial}{\partial x} (vf) + \frac{\partial}{\partial v} \left(\left(\frac{\partial \Phi}{\partial x} - \mathcal{D} \right) f \right) = 0, \quad (25)$$

where \mathcal{D} is given by Eq.(19). The equations of motion are then given by

$$\begin{aligned} \frac{dx_j}{dt} &= v_j, \\ \frac{dv_j}{dt} &= \frac{\partial \Phi}{\partial x} \Big|_{x_j} - \mathcal{D}(x_j, v_j). \end{aligned}$$

The conservation properties associated with the system Eqs.(22-24) can be derived by taking velocity moments of the Vlasov equation. These conservation properties are given by (see Appendix A):

$$\frac{\partial \langle n \rangle_x}{\partial t} \equiv \frac{\partial N}{\partial t} = 0, \quad (26)$$

$$\frac{\partial}{\partial t} \langle \Gamma \rangle_x = -\nu_{ei} \langle \Gamma \rangle_x , \quad (27)$$

and

$$\frac{\partial}{\partial t} (K + U) = -\nu_{ei} (2K - N) , \quad (28)$$

where $\Gamma = \int_{-\infty}^{+\infty} v f dv$ is the particle flux, $U = \frac{1}{2} \langle (\partial\Phi/\partial x)^2 \rangle_x$ is the potential energy, $K = \left\langle \int_{-\infty}^{+\infty} (v^2/2) f dv \right\rangle_x$ is the kinetic energy, $\langle \bullet \rangle_x$ denotes spatial average. Eqs.(26-28) show that in the absence of collisional dissipation the particle number, the total momentum and the total energy $E = K + U$ are conserved. For the specific collision operator used in this paper only the particle number N is conserved when $\nu_{ei} \neq 0$. Eq.(27) shows that the total momentum decays in time according to

$$\langle \Gamma \rangle_x (t) = \langle \Gamma \rangle_x (0) e^{-\nu_{ei} t} . \quad (29)$$

Integrating Eq.(28) and taking into account Eq.(26) the following quantity should vanish:

$$\delta E \equiv \left| K(t) - K(0) + U(t) - U(0) + 2\nu_{ei} \int_0^t K(t') dt' - \nu_{ei} N(0)t \right| . \quad (30)$$

Fig. 9 shows the time evolution of the total momentum for a system of length $L = 8$ and a number of markers $N = 6765$. The number of grid points is $N_g = 64$, the collision frequency is $\nu_{ei} = 0.2$ and the time step is $\Delta t = 0.025$. The plain line is the exact solution [Eq.(29)] whereas the dotted line represents the time evolution of the total momentum using the Monte Carlo operator; we note that the decay rate for $\langle \Gamma \rangle_x$ exceeds the theoretical value. The dashed line is for the case of the deterministic collision operator; the time evolution of $\langle \Gamma \rangle_x$ is in excellent agreement with the theoretical value.

The most dramatic difference between the Monte Carlo method and the deterministic method is with respect to the overall energy conservation. If the simulated plasma were to conserve energy exactly then $\delta E(t) = 0$ [Eq.(30)] at any time t . However, apart from the well-known causes for the nonconservation of energy (finite number of markers, finite spatial grid size, cumulative errors in the integration of the equations of motion, etc.) the method of implementation of the collision operator also plays an important role. This is illustrated in Fig. 10 where the variation of energy δE is depicted for the same parameters

and initial conditions as in Fig. 9. The Monte Carlo implementation of the collision operator (dotted line) yields a secular increase in δE . However, the deterministic collision operator results in a much smaller nonconservation of energy. More importantly, δE saturates for the deterministic collision operator whereas it does not for the case of a Monte Carlo collision operator.

V. CONCLUSIONS

In this paper a new method to implement collision operators in particle-in-cell simulations has been discussed. The main idea behind the new method is to write a given collision operator as a conservation equation in velocity space which can then be naturally included in the Lagrangian formulation that pertain to the collisionless dynamics; as a result, no random numbers are needed in the implementation. One major advantage of the low-noise collision operator is that the conservation properties of the simulated plasma are considerably improved. In addition, the method can be easily generalized to more complex collision operators such as Fokker-Planck collision operators.

APPENDIX A: CONSERVATION PROPERTIES OF THE VLASOV-POISSON SYSTEM

In this Appendix, we derive the conservation properties of the Vlasov-Poisson system given by

$$\frac{\partial f}{\partial t} + v \frac{\partial f}{\partial x} + \frac{\partial \Phi}{\partial x} \frac{\partial f}{\partial v} = C(f) , \quad (\text{A1})$$

where

$$C(f) = \frac{\partial}{\partial v} \left(\nu_{ei} \frac{\partial f}{\partial v} + \nu_{ei} v f \right) , \quad (\text{A2})$$

$$\frac{\partial^2 \Phi}{\partial x^2} = \rho \equiv \int_{-\infty}^{+\infty} f dv - 1 = n - 1 . \quad (\text{A3})$$

It is convenient to introduce the velocity average operator

$$\langle \bullet \rangle_v \equiv \int_{-\infty}^{+\infty} \bullet dv , \quad (\text{A4})$$

and the spatial average operator

$$\langle \bullet \rangle_x \equiv \frac{1}{L} \int_0^L \bullet dx , \quad (\text{A5})$$

Note that

$$\left\langle \frac{\partial g}{\partial x} \right\rangle_x = \left\langle \frac{\partial g}{\partial v} \right\rangle_v = 0 , \quad (\text{A6})$$

for any physical quantity $g = g(x, v)$. Multiply Eq.(A1) by v^k and operate with $\langle \bullet \rangle_v$, one gets after a few integration by parts

$$\frac{\partial}{\partial t} M_k + \frac{\partial}{\partial x} M_{k+1} - k \frac{\partial \Phi}{\partial x} M_{k-1} = D_k , \quad (\text{A7})$$

where

$$M_k \equiv \int_{-\infty}^{+\infty} v^k f dv \quad \text{for } k = 0, 1, 2, \dots \quad (\text{A8})$$

is the velocity moment of order k and

$$D_k \equiv -\nu_{ei} k \left[\underbrace{M_k}_{\text{drag}} - \underbrace{(k-1)M_{k-2}}_{\text{diffusion}} \right] . \quad (\text{A9})$$

accounts for the collisional dissipation. The spatial average of Eq.(A7) is

$$\frac{\partial}{\partial t} \langle M_k \rangle_x - k \left\langle \frac{\partial \Phi}{\partial x} M_{k-1} \right\rangle_x = \langle D_k \rangle_x \quad (\text{A10})$$

We now use the standard notation for the density, $n \equiv M_0$, the particle flux, $\Gamma \equiv M_1$, and the kinetic energy, $\mathcal{E} \equiv M_2/2$. It is easy from the definition (A9) that $D_0 = 0$, $D_1 = -\nu_{ei}\Gamma$ and $D_2 = -2\nu_{ei}(2\mathcal{E} - n)$. Equation (A10) for $k = 0$ shows that the total number of particles is conserved

$$\frac{\partial}{\partial t} \langle n \rangle_x \equiv \frac{\partial N}{\partial t} = 0. \quad (\text{A11})$$

The spatial average of the first-order moment of the collisional Vlasov equation is

$$\frac{\partial}{\partial t} \langle \Gamma \rangle_x - \left\langle n \frac{\partial \Phi}{\partial x} \right\rangle_x = \langle D_1 \rangle_x \quad (\text{A12})$$

where, from Poisson equation (A3), the density is given by $n = 1 + \partial^2 \Phi / \partial x^2$. It follows that

$$\begin{aligned} \left\langle n \frac{\partial \Phi}{\partial x} \right\rangle_x &= \left\langle \frac{\partial \Phi}{\partial x} \frac{\partial^2 \Phi}{\partial x^2} \right\rangle_x, \\ &= \frac{1}{2} \left\langle \frac{\partial}{\partial x} \left(\frac{\partial \Phi}{\partial x} \right)^2 \right\rangle_x, \\ &= \frac{1}{2} \left\langle \frac{\partial E^2}{\partial x} \right\rangle_x = 0, \end{aligned}$$

since the system is spatially periodic. Eq.(A12) then becomes

$$\frac{\partial}{\partial t} \langle \Gamma \rangle_x = -\nu_{ei} \langle \Gamma \rangle_x \quad (\text{A13})$$

which can be integrated directly to give

$$\langle \Gamma \rangle_x = \langle \Gamma \rangle_x(0) \exp(-\nu_{ei}t). \quad (\text{A14})$$

In the absence of collisions ($\nu_{ei} = 0$), the total momentum of the system is conserved. The spatial average of the second-order velocity moment of the collisional Vlasov equation is

$$\frac{\partial}{\partial t} \langle \mathcal{E} \rangle_x - \left\langle \Gamma \frac{\partial \Phi}{\partial x} \right\rangle_x = -\nu_{ei} (2 \langle \mathcal{E} \rangle_x - \langle n \rangle_x). \quad (\text{A15})$$

Using

$$\left\langle \Gamma \frac{\partial \Phi}{\partial x} \right\rangle_x = - \left\langle \Phi \frac{\partial \Gamma}{\partial x} \right\rangle_x$$

and the continuity equation [$k = 0$ in Eq.(A7)]

$$\frac{\partial n}{\partial t} + \frac{\partial \Gamma}{\partial x} = 0 ,$$

we obtain

$$\left\langle \Gamma \frac{\partial \Phi}{\partial x} \right\rangle_x = \left\langle \Phi \frac{\partial n}{\partial t} \right\rangle_x ,$$

whereas the time derivative of Eq.(A3) yields

$$\frac{\partial n}{\partial t} = \frac{\partial}{\partial t} \frac{\partial^2 \Phi}{\partial x^2} .$$

It follows that

$$\begin{aligned} \left\langle \Gamma \frac{\partial \Phi}{\partial x} \right\rangle_x &= \left\langle \Phi \frac{\partial}{\partial t} \frac{\partial^2 \Phi}{\partial x^2} \right\rangle_x \\ &= \left\langle -\Phi \frac{\partial}{\partial x} \frac{\partial E}{\partial t} \right\rangle_x \quad (E = -\partial \Phi / \partial x) \\ &= \left\langle -\Phi \frac{\partial \eta}{\partial x} \right\rangle_x \quad (\eta = \partial E / \partial t) \\ &= \left\langle \eta \frac{\partial \Phi}{\partial x} \right\rangle_x \\ &= \langle -\eta E \rangle_x \\ &= -\frac{1}{2} \left\langle \frac{\partial E^2}{\partial t} \right\rangle_x . \end{aligned}$$

We can write Eq.(A15) as

$$\frac{\partial}{\partial t} (K + U) = -\nu_{ei} (2K - N) , \tag{A16}$$

where, as before, $N \equiv \langle n \rangle_x$ is the total number of particles,

$$U \equiv \frac{1}{2} \langle E^2 \rangle_x$$

is the field energy, and

$$K \equiv \langle \mathcal{E} \rangle_x$$

is the kinetic energy.

Acknowledgments This research was supported by Contract No. DE-AC02-CH0-3073 and the Scientific Discovery through Advanced Computing (SciDAC) initiative (U.S. Department of Energy).

-
- [1] C.K. Birdsall and A.B. Langdon, *Plasma Physics via Computer Simulations*, McGraw-Hill, New York (1985).
- [2] R.W. Hockney and J.W. Eastwood, *Computer Simulations using Particles*, McGraw-Hill, New York (1981).
- [3] J.L.V. Lewandowski, *Phys. of Plasmas*, **10**, 3204 (2003).
- [4] R. Shanny, J.M. Dawson and J.M. Greene, *Phys. Fluids*, **10**, 1281 (1967).
- [5] J.L.V. Lewandowski, *Can. J. Phys.*, **81**, 1331 (2003).
- [6] A. Chorin, *J. Fluid Mech.*, **57**, 785 (1973).
- [7] P.J. Catto and K.T. Tsang, *Phys. Fluids*, **20**, 396 (1977).
- [8] X.Q. Xu and M.N. Rosenbluth, *Phys. Fluids B***3**, 627 (1991).
- [9] T. Takizuka and H. Abe, *J. Comput. Phys.* **8**, 19 (1977).
- [10] R.J. Procassini and C.K. Birdsall, *Nucl. Fusion* **30**, 2329 (1990).
- [11] S. Ma, R.D. Sydora and J.M. Dawson, *Comput. Phys. Commun.* **77**, 190 (1993).
- [12] J.L.V. Lewandowski, *J. of Scientific Computing* , **21**(2), 174 (2004).
- [13] W.S Press, S.A. Teukolsky, W.T. Vetterling and B.P. Flannery, *Numerical Recipes in Fortran*, Cambridge University Press, New York (1992).

Figure 1 Approximation of the function $f(x) = xe^{-x^2}$ (plain line) based on a set of $N = 32$ markers. The dotted (dashed) line is for the case of uniform (nonuniform) spatial loading. The shape function is a quadratic polynomial [$S(x) = S_3(x)$; see Eq.(12)] with parameter $\epsilon = 0.1$.

Figure 2 Approximation of the function $f(x) = xe^{-x^2}$ (plain line) based on a set of $N = 32$ markers. The dotted (dashed) line is for the case of uniform (nonuniform) spatial loading. The shape function is a quartic polynomial [$S(x) = S_4(x)$; see Eq.(12)] with parameter $\epsilon = 0.1$.

Figure 3 Approximation of the function $f(x) = xe^{-x^2}$ (plain line) based on a set of $N = 32$ markers. The dotted (dashed) line is for the case of uniform (nonuniform) spatial loading. The shape function is based on a quartic polynomial and a Gaussian function [$S(x) = S_6(x)$; see Eq.(12)] with parameter $\epsilon = 0.1$.

Figure 4 Approximation of the function $f(x) = xe^{-x^2}$ (plain line) based on a set of $N = 32$ markers. The dotted (dashed) line is for the case of uniform (nonuniform) spatial loading. The shape function is a quartic polynomial [$S(x) = S_4(x)$; see Eq.(12)] with parameter $\epsilon = 0.2$.

Figure 5 Exact (plain line: $t = 2.0$; dotted line: $t = 4.0$) and approximate (triangles: $t = 2.0$; squares: $t = 4.0$) solutions of the diffusion equation based on a set of $N = 100$ markers. The initial condition is a square profile, Eq.(15). The shape function is a superGaussian [Eq.(16)]. Other parameters are: $\Delta t = 0.01$, $\epsilon = 1/3$ and $L = 14.0$.

Figure 6 Collisional relaxation of an initial square distribution function (plain line) towards a Maxwellian distribution (dashed line) using the Monte Carlo method. The parameters are: $N = 200$ (number of markers), $\Delta t = 0.1$ (time step), $N_s = 600$ (number of time steps) and $\nu_{ei} = 0.5$ (collision frequency). The final distribution, shown as a dotted line, has been reconstructed on a fixed grid with $N_g = 500$ grid points.

Figure 7 Collisional relaxation of an initial square distribution function (plain line) towards a Maxwellian distribution (dashed line) using the deterministic marker method. The parameters are: $N = 200$ (number of markers), $\Delta t = 0.1$ (time step), $N_s = 600$ (number of time steps) and $\nu_{ei} = 0.5$ (collision frequency). The final distribution,

shown as a dotted line, has been reconstructed on a fixed grid with $N_g = 500$ grid points.

Figure 8 Final distribution function using the deterministic marker method. The plain line represents the Maxwellian distribution. The triangles represent the position of the markers. The parameters are: $N = 200$ (number of markers), $\Delta t = 0.1$ (time step), $N_s = 600$ (number of time steps) and $\nu_{ei} = 0.5$ (collision frequency). The final distribution, shown as a dotted line, has been reconstructed on a fixed grid with $N_g = 500$ grid points.

Figure 9 Time evolution of the total momentum Γ for a simulation with $N = 6765$ markers, system length $L = 8$ and number of grid points $N_g = 64$. The time step is $\Delta t = 0.025$ and the collision frequency is $\nu_{ei} = 0.2$. The plain line is the theoretical value, the dotted line is for the case of a Monte Carlo collision whereas the dashed is for the case of a deterministic collision operator.

Figure 10 Variation of total energy δE , defined in Eq.(30), as a function of time for the same simulation as in Fig. 9. The dotted line is for the case of Monte Carlo collision operator whereas the plain line is for the case of a deterministic collision operator. The theoretical value is $\delta E \equiv 0$.

Figure 1 Lewandowski

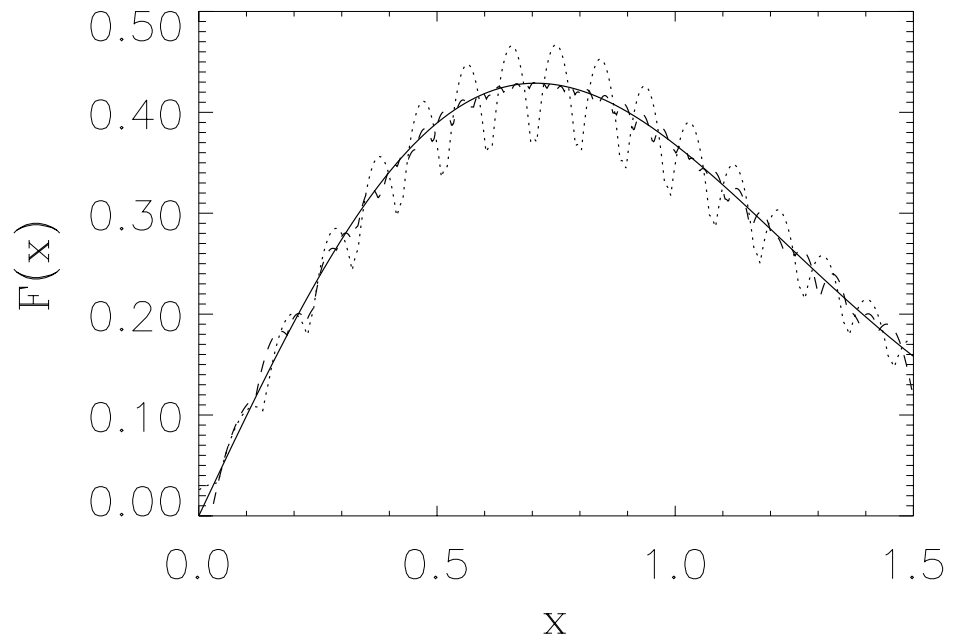


Figure 2 Lewandowski

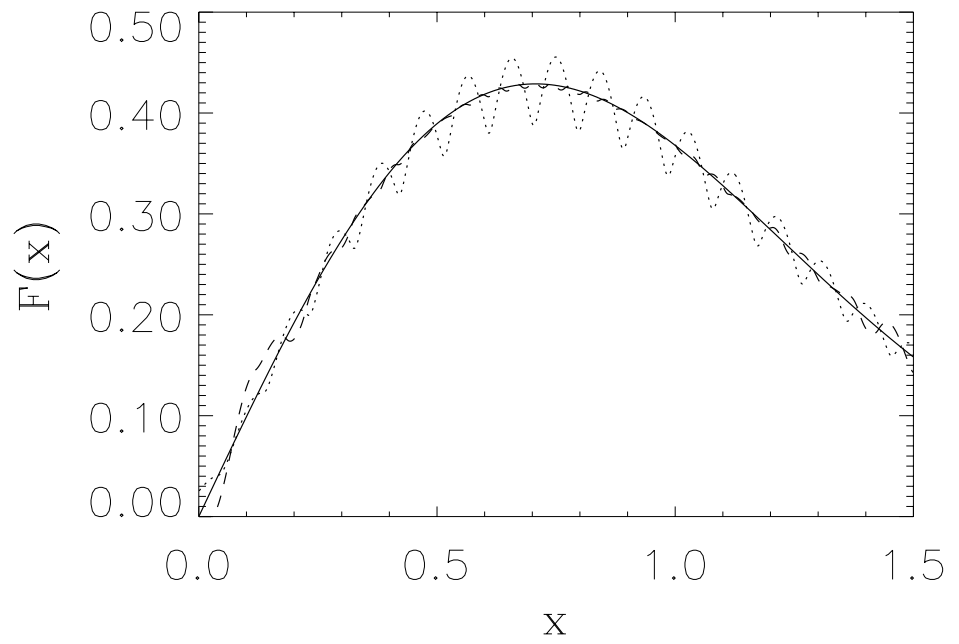


Figure 3 Lewandowski

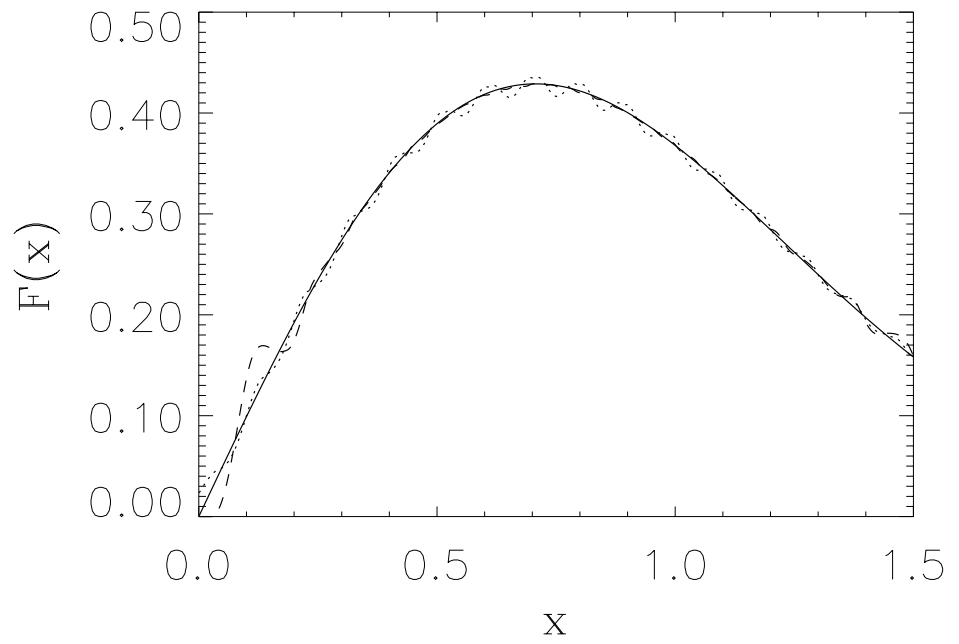


Figure 4 Lewandowski

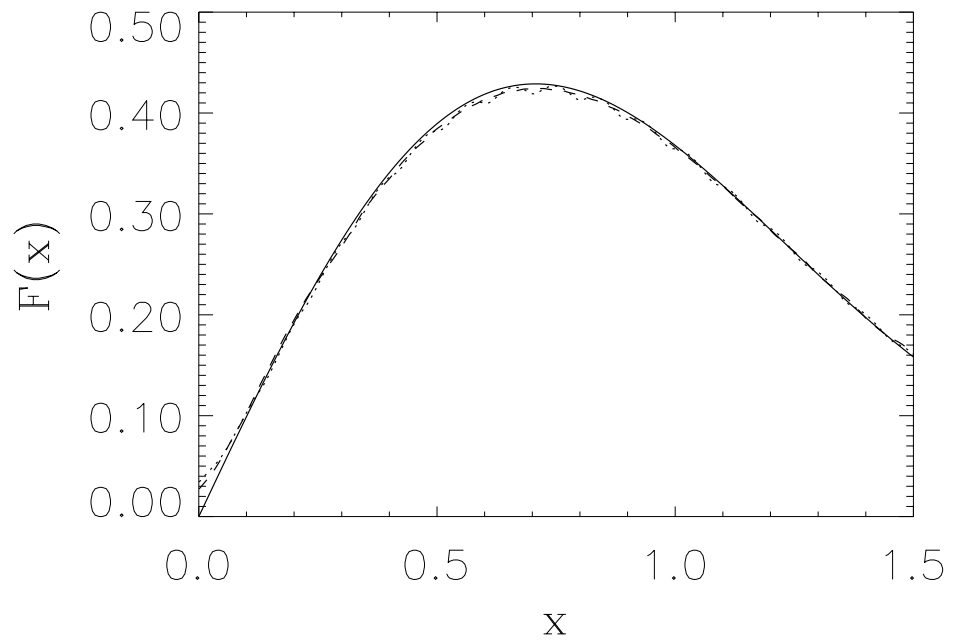


Figure 5 Lewandowski

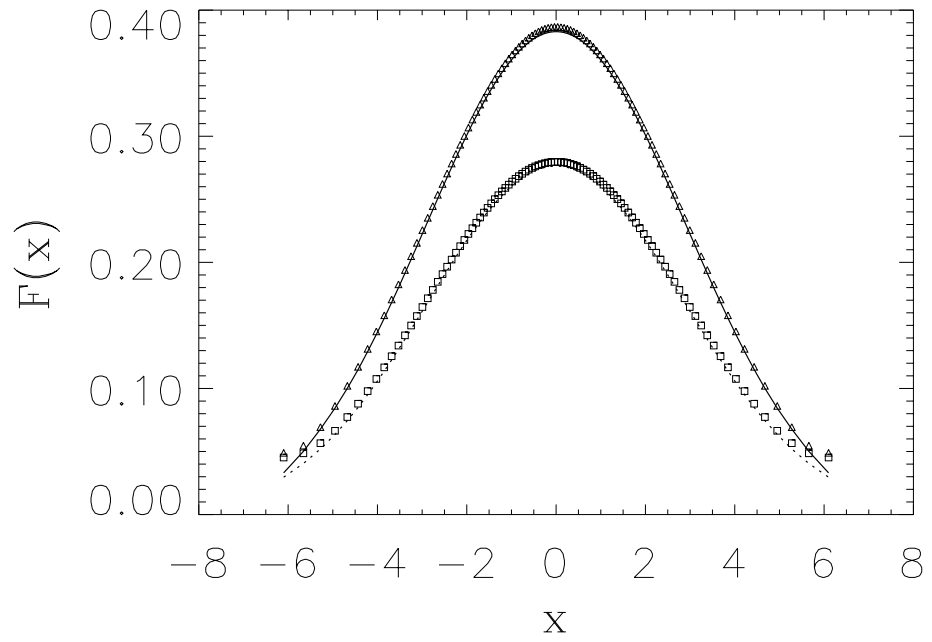


Figure 6 Lewandowski

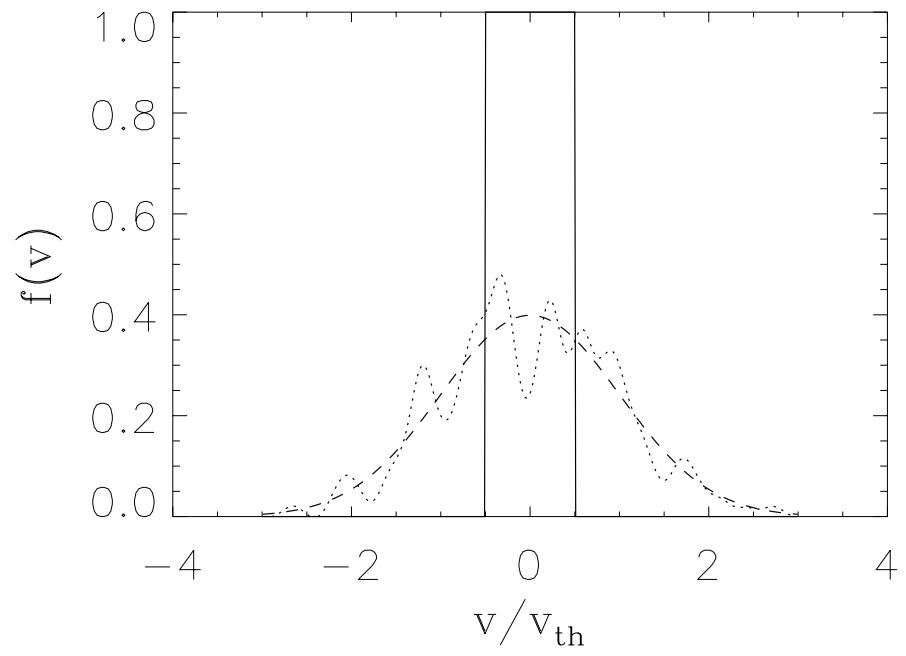


Figure 7 Lewandowski

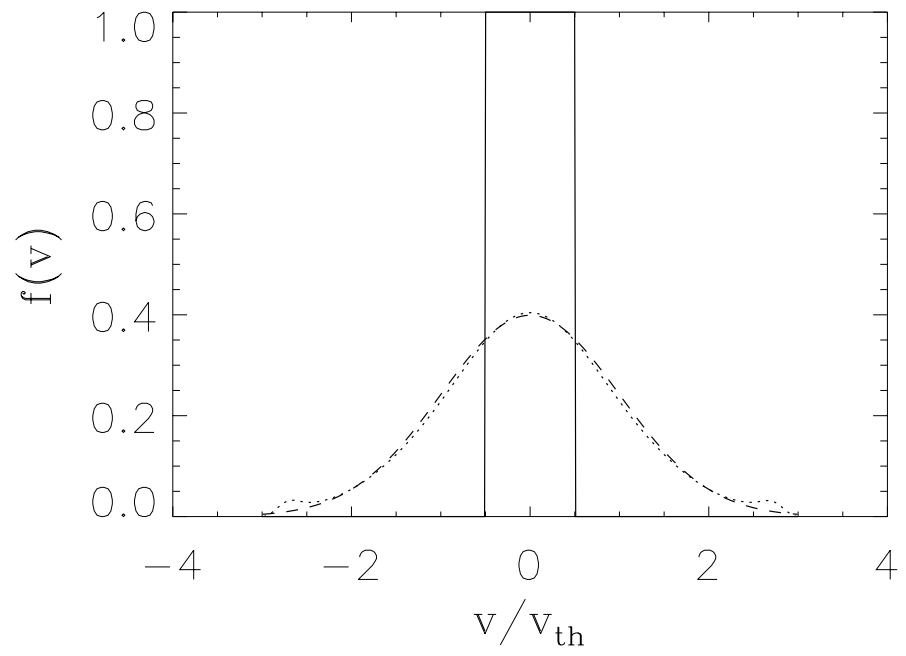


Figure 8 Lewandowski

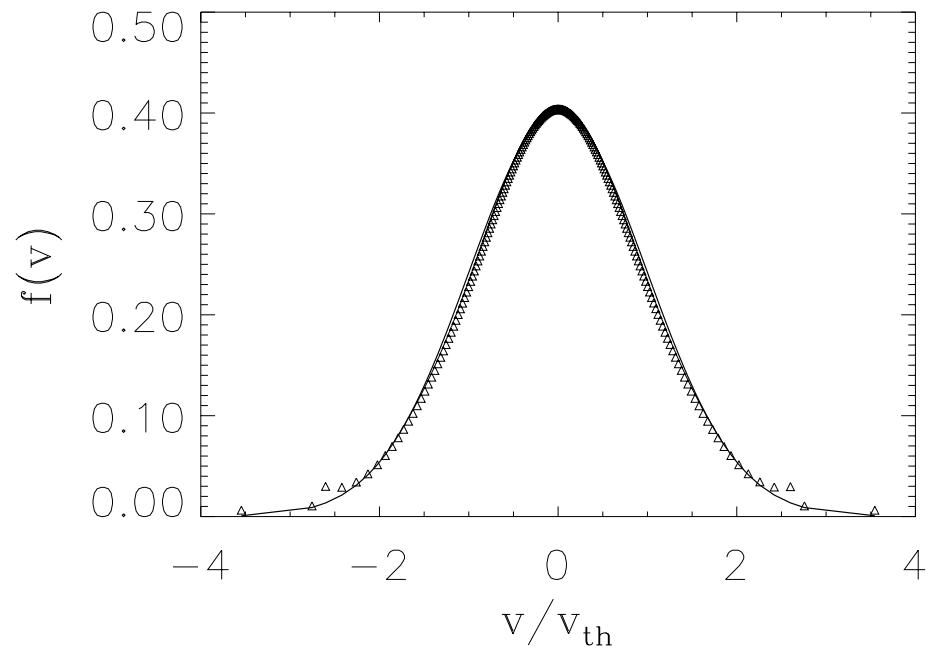


Figure 9 Lewandowski

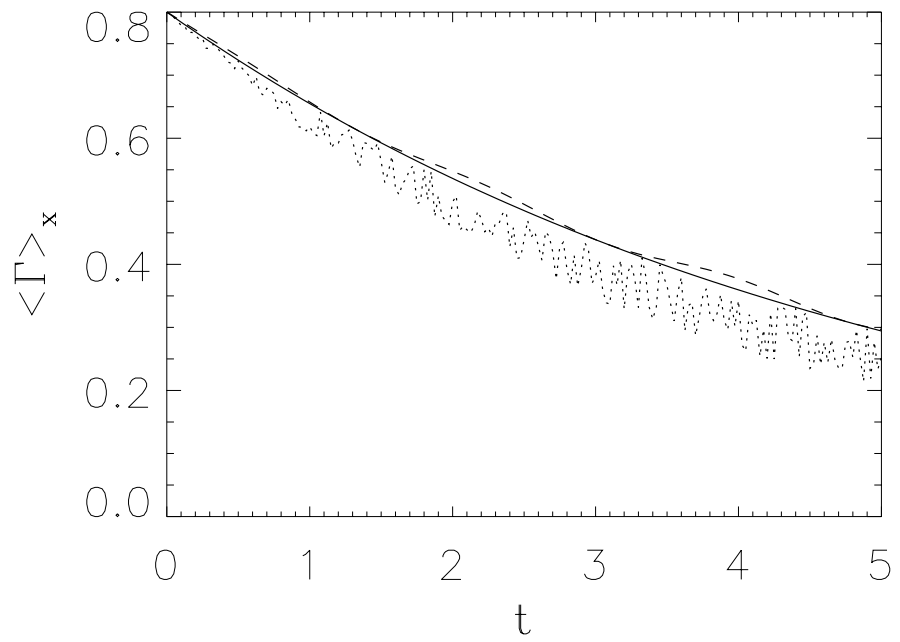
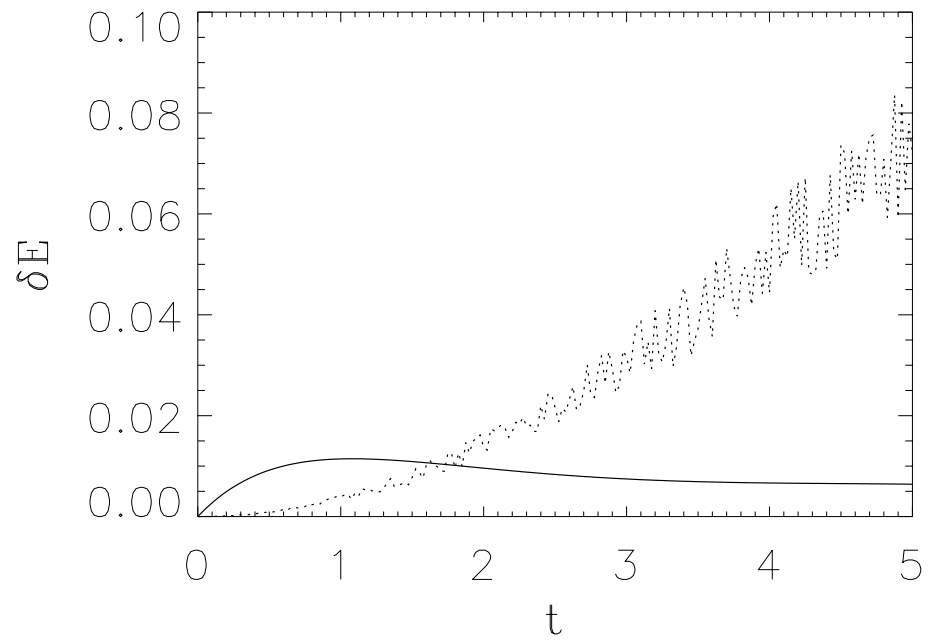


Figure 10 Lewandowski



External Distribution

Plasma Research Laboratory, Australian National University, Australia
Professor I.R. Jones, Flinders University, Australia
Professor João Canalle, Instituto de Fisica DEQ/IF - UERJ, Brazil
Mr. Gerson O. Ludwig, Instituto Nacional de Pesquisas, Brazil
Dr. P.H. Sakanaka, Instituto Fisica, Brazil
The Librarian, Culham Science Center, England
Mrs. S.A. Hutchinson, JET Library, England
Professor M.N. Bussac, Ecole Polytechnique, France
Librarian, Max-Planck-Institut für Plasmaphysik, Germany
Jolan Moldvai, Reports Library, Hungarian Academy of Sciences, Central Research Institute
for Physics, Hungary
Dr. P. Kaw, Institute for Plasma Research, India
Ms. P.J. Pathak, Librarian, Institute for Plasma Research, India
Dr. Pandji Triadyaksa, Fakultas MIPA Universitas Diponegoro, Indonesia
Professor Sami Cuperman, Plasma Physics Group, Tel Aviv University, Israel
Ms. Clelia De Palo, Associazione EURATOM-ENEA, Italy
Dr. G. Grosso, Istituto di Fisica del Plasma, Italy
Librarian, Naka Fusion Research Establishment, JAERI, Japan
Library, Laboratory for Complex Energy Processes, Institute for Advanced Study,
Kyoto University, Japan
Research Information Center, National Institute for Fusion Science, Japan
Dr. O. Mitarai, Kyushu Tokai University, Japan
Dr. Jiangang Li, Institute of Plasma Physics, Chinese Academy of Sciences,
People's Republic of China
Professor Yuping Huo, School of Physical Science and Technology, People's Republic of China
Library, Academia Sinica, Institute of Plasma Physics, People's Republic of China
Librarian, Institute of Physics, Chinese Academy of Sciences, People's Republic of China
Dr. S. Mirnov, TRINITI, Troitsk, Russian Federation, Russia
Dr. V.S. Strelkov, Kurchatov Institute, Russian Federation, Russia
Professor Peter Lukac, Katedra Fyziky Plazmy MFF UK, Mlynska dolina F-2,
Komenskeho Univerzita, SK-842 15 Bratislava, Slovakia
Dr. G.S. Lee, Korea Basic Science Institute, South Korea
Dr. Rasulkhozha S. Sharafiddinov, Theoretical Physics Division, Institute of Nuclear Physics,
Uzbekistan
Institute for Plasma Research, University of Maryland, USA
Librarian, Fusion Energy Division, Oak Ridge National Laboratory, USA
Librarian, Institute of Fusion Studies, University of Texas, USA
Librarian, Magnetic Fusion Program, Lawrence Livermore National Laboratory, USA
Library, General Atomics, USA
Plasma Physics Group, Fusion Energy Research Program, University of California
at San Diego, USA
Plasma Physics Library, Columbia University, USA
Alkesh Punjabi, Center for Fusion Research and Training, Hampton University, USA
Dr. W.M. Stacey, Fusion Research Center, Georgia Institute of Technology, USA
Dr. John Willis, U.S. Department of Energy, Office of Fusion Energy Sciences, USA
Mr. Paul H. Wright, Indianapolis, Indiana, USA

The Princeton Plasma Physics Laboratory is operated
by Princeton University under contract
with the U.S. Department of Energy.

Information Services
Princeton Plasma Physics Laboratory
P.O. Box 451
Princeton, NJ 08543

Phone: 609-243-2750
Fax: 609-243-2751
e-mail: pppl_info@pppl.gov
Internet Address: <http://www.pppl.gov>